https://doi.org/10.5194/egusphere-2023-2824
Preprint. Discussion started: 23 January 2024

Predicting the productivity of Alpine grasslands using remote sensing information

Saverio Vicario[1], Marta Magnani[2,3,4], Maria Adamo[1], Gianna Vivaldo[3,5], Chiara Richiardi[1,6], Mariasilvia Giamberini[5], and Antonello Provenzale[5]

[1]Via Orabona 4 Bari 70125, Istituto sull'Inquinamento Atmosferico - Consiglio Nazionale delle Ricerce C/O "M. Merlin" Dip. Fisica Univ. Bari
[2]Via Valperga Caluso 35 - 10125 Torino, Italy, Istituto di Geoscienze e Georisorse - Consiglio Nazionale delle Ricerce
[3]90133 Palermo, Italy, National Biodiversity Future Center
[4]Via Pietro Giuria 1 - 10125 Torino, Italy, INFN
[5]Via Giuseppe Moruzzi 1 - 56124 Pisa, Istituto di Geoscienze e Georisorse - Consiglio Nazionale delle Ricerce
[6]Via Pier Andrea Mattioli 25, 10125 Turin, Italy - Department of Life Sciences and Systems Biology, University of Torino

Correspondence: saverio vicario (saverio.vicario@cnr.it)

Abstract. Gross primary productivity (GPP) is a crucial variable for ecosystem dynamics, and it can significantly vary on the small spatial scales of vegetation and environmental heterogeneity. This is especially true for mountain ecosystems, which pose severe difficulties to field monitoring. In addition, the specificity of such ecosystems and the extreme abiotic conditions that they experience often make global and regional models unsuited to predictions. In this case, remote sensing products offer the opportunity to explore the productivity of vegetation communities in remote areas such as Alpine grasslands all year round, and empirical models can help in the challenge of modelling Alpine GPP. Along these lines, we took a hybrid approach, blending several remote sensing data sources (such as a high-definition digital terrain model and moderate- and high- resolution satellite products such as MODIS and Sentinel 2) and gridded datasets such as ERA5 with *in situ* measurements to implement a specific empirical model. The resulting remote-sensing-based model developed here was suited to represent the measured primary productivity in different areas within a high-altitude grassland at the Nivolet plain, in the north-western Italian Alps at 2700-2500m amsl. A cross-validation approach allowed us to evaluate to what extent a single empirical model could represent diverse communities and different abiotic factors found in these areas. We finally identified the ratio between MCARI2 and MSAVI2 as a good predictor of light use efficiency, a key factor in the empirical model, probably due to its good correlation with the leaves phenological status, inasmuch it estimates the ratio between chlorophyll and the ensemble of leaf pigments.

1 Introduction

In terrestrial ecosystems, plant primary productivity associated with photosynthesis is an essential variable for climate and biodiversity studies (de Paula et al., 2020; Lehmann et al., 2020). Photosynthesis is responsible for the removal of a large

https://doi.org/10.5194/egusphere-2023-2824
Preprint. Discussion started: 23 January 2024

fraction of carbon dioxide (CO_2) from the atmosphere (Friedlingstein et al., 2022) and it is the main process through which new energy enters the food webs, thus being an important regulator of ecosystem functions and biodiversity.

Although primary productivity is a relevant variable in many types of studies, the spatial and temporal resolution needed in the various applications is rather different. Current regional climate models are geared to have grid cell resolution of a few kilometres or more, and require average values on such scales (Wiltshire et al., 2021; Balsamo et al., 2018). On the other hand, ecological and biodiversity studies ideally require primary productivity information to be available at the level of communities. In very heterogeneous grasslands, such as those found in mountain environments, this implies a spatial resolution of few tens of square meters (Li et al., 2019). These widely variable spatial scales are usually addressed by quite different methods, pointing to the necessity of upscaling-dowscaling techniques that can link small scale CO_2 flux estimates and large-scale models.

In this work, we built regressive models of measured Gross Primary Productivity (GPP) using remote sensing products. To model GPP, we take the general approach of the Monteith light-use efficiency model (Rossini et al., 2012) in which GPP is computed using the incident photo-synthetically active radiation (PAR_{inc}), the fraction of PAR_{inc} that it is absorbed ($fAPAR$) and the Light Use Efficiency (LUE) that converts the energy absorbed in the actual work of fixing carbon dioxide. The PAR_{inc} has two sources, namely the direct radiation from the sun and the indirect one scattered from the atmosphere. For the present work we disregarded a third source, the indirect radiation reflected from other surrounding surfaces.

Both sources are (complicated) fractions of the top-of-atmosphere radiation, while this latter can be easily calculated from astronomical and geographical information. The fAPAR is usually estimated from vegetation indices or, more recently, by using machine learning approaches, such as the system included in sen2core (Main-Knorn et al., 2017). The accuracy of such an estimate (hereafter called FAPAR) for these two alternative approaches depends on the type of vegetation index and its relationship to the number of photons absorbed by the photosystem, or the training set used in the machine learning approach, respectively. The estimate of LUE is more problematic. In biochemical studies, it encompasses all potential energetic losses of the different reactions included in photosythesis, including the antenna complex during the dissipation state (xantophyll photoprotection effect), the fluorescence and heat dissipation of photosystems, the loss of energy of the electron transport system through proton leakage across membranes, generated by changes in temperature, and the variable functioning of Rubisco that oscillates between a proper carbon-fixing Calvin cycle and a carbon-releasing photorespiration owing to drought or/and high temperature (Porcar-Castell et al., 2014). This latter reaction, photorespiration, is not included in the estimate of GPP in studies focusing on carbon budget, given that the carbon dioxide produced by photorespiration is accounted for in the general plant respiration processes.

Another approach to estimate LUE, which is often used in climate modelling studies, is based on Plant Functional Types (PFT) (Poulter et al., 2015). In this case, a limited number of PFT classes are defined and a model that links air temperature, soil temperature and air humidity to an estimate of LUE is assumed for each class. In this approach, photorespiration is included in the LUE estimates, distinguishing between C3 grasses that display this phenomenon and C4 grasses that do not show it.

In the nineties, the photochemical radiation index (PRI) has been proposed as an alternative to the PFT-approach to estimate LUE from remote sensing products. The PRI targets the transformation of the pigment violaxanthin to zeaxanthin, a photoprotective compound that releases the PAR photon energy as heat, within the xanthophyll cycle. The zeaxanthin produces a

https://doi.org/10.5194/egusphere-2023-2824
Preprint. Discussion started: 23 January 2024

distinctive spectral signal at 531 nm and, after several testing (Gamon et al., 1992) to produce a normalized index, the reference band was selected to be centered at 570 nm. Middleton et al (Middleton et al., 2016) successfully adapted the PRI approach to MODIS sensors, using the band 11 as the main signal, with 1 km and 526–536 nm for spatial and spectral resolution respectively, and the band 1 (whose spatial and spectral resolutions are respectively 250 m and 620–670 nm) as reference (Middleton et al., 2016). These authors further noted that a specific geometry between sun and satellite is necessary to obtain correct measures of PRI.

Albeit the difficulties in implementing the Monteith approach mentioned above, we did not adopt the alternative strategy based on the use of Sun Induced Fluorescence (SIF). The SIF method measures fluorescence emissions from both photosystems, trying to infer the number of photons that reach the photosystem by assuming that the fluorescence rate is constant. As such, this method measures directly GPP as a whole. However, the actual measuring of SIF is complex, owing to the low intensity of the signal and the partial re-absorption of the signal from the canopy (Yang et al., 2020).

In this work, we model the Gross Primary Productivity of an Alpine grassland using remote sensed drivers and fitting the model to a multi-annual *in situ* measurement dataset. Because an approach based on generic plant types (such as the PFT) or an average biome response (i.e "grassland model") is not accurate enough for community-scale estimates and for this particular type of high-altitude Alpine vegetation, we empirically fit the parameters of the Light Use Efficiency model. In the modelling work, we used only open remote sensing products, trying to balance the spectral, temporal and spatial resolution.

2 Materials and Methods

2.1 Study Area and *in situ* data

The *in situ* data used to validate the remote-sensing estimates were acquired at the Nivolet Plain, Gran Paradiso National Park (GPNP), in the north-western Italian Alps (Fig. 2). The GPNP is the oldest Italian National Park, established in 1922 for the conservation of the Alpine ibex, *Capra ibex*, and its mountain habitat (www.pngp.it). The park covers a surface of 720 km^2 (between 45°25' and 45°45' N, and 7° and 7°30' W) and has an elevation range between 800 and 4061 m a.s.l.. It includes five valleys (i.e., Rhêmes, Valsavarenche, Cogne, Soana and Orco) located between the Val d'Aosta (52% of the park area) and Piedmont (48%) regions, at the border with France.

The park area is covered with 55% grasslands, 18% forests and shrubs, 20% bare rocks, and 7% permanent snow and ice (Buchhorn et al., 2020; Filippa et al., 2022), and it is part of the European LTER network (https://deims.org/e33c983a-19ad-4f40-a6fd-1210ee0b3a4b).

From November to early-mid June, at elevations above 2000 m a.s.l., the soil is usually covered with snow, with maximum snow depth higher than 250 cm in the years 2017-2019, as measured by the meteorological station at Lake Serru (2450 m a.s.l.), close to the Nivolet Plain. At this station, the mean annual precipitation over the period 1962-2020 was 1185 mm/year. The mean daily temperature during June-October ranged from 3 to 12 °C (5th and 95th quantiles, respectively).

The Nivolet Plain is a high-altitude valley whose floor goes from about 2650 meters (at the Col del Nivolet pass) to 2400 meters at its outlet, and it is characterized by a meandering stream flowing towards nord east, and then rushing down through several waterfalls to Valsavarenche, at an elevation of about 2000 meters. The flanks of the Nivolet Plain rise rapidly to much

https://doi.org/10.5194/egusphere-2023-2824
Preprint. Discussion started: 23 January 2024

higher elevations, and are spotted by several lakes of glacial origin. The metamorphic bedrock of the sampling sites belongs to the Gran Paradiso Unit, composed of abundant gneisses and minor quartzites, dolostones and marbles, and to the oceanic Piedmont-Ligurian zone, consisting of calcschists with serpentinites and metabasites (Piana et al., 2017). Quaternary glacial and alluvial deposits variably cover these rocks.

Above treeline, the high-altitude grasslands studied here are composed of typical Alpine species, such as *Nardus sp.*, *Festuca sp.* and *Carex curvula* (Danna et al., 2022), and pioneer species, such as *Saxifraga oppositifolia*, *Silene acaulis* and *Poa alpina*, are common in glacier forelands (Mainetti et al., 2021).

The flux data have been measured in five square plots of about 10 x 10 meters, located either at the Nivolet floor or along its flanks, that were regularly sampled since 2017. Two of the plots were at about 2700 m of elevation on the north-western side of the valley, while the other two were at about 2450 m on the south-eastern side of the valley. Four of the five plots were on different types of rock substrate, and all were in the same watershed. The study plots represent fairly well the main configurations of soil type, exposure, and water availability present within the valley and typical of high-altitude Alpine grasslands. In all plots, NEE (Net Ecosystem Exchange) and ER (Ecosystem Respiration) were measured using the non-steady-state closed dynamic accumulation chamber method (Baneschi et al., 2023), in addition to several ancillary variables (incident total radiation, air and soil temperature and humidity, air pressure). Four of these plots have been sampled since 2017, while one plot (called ECT in Fig. 2) has been included in 2020. Every 10 to 15 days, in each of the plots, flux measurements were performed in 15 to 20 individual points that were randomly distributed over the plot area. The full sampling of a plot required from 1.5 to 2 hours, which have been accounted for when synchronising data from other sources. Further details about the measurement procedure can be found in Magnani et al. (2020); Lenzi et al. (2023).

2.2 Remote sensing GPP estimates

The basic formula used in remote sensing approaches for the computation of gross primary production is the following:

$$GPP = APAR \cdot LUE \tag{1}$$

where APAR is the amount of photosynthetically active radiation absorbed by the plants and LUE is the Light Use Efficiency in transforming APAR energy in work that fix carbon dioxide in carbon chain. Generally, the APAR is split into incident PAR or PAR_{inc}, and $fAPAR$ that is the fraction of absorbed PAR_{inc}; while the LUE varies for different type of plants but also depends on the physiological status and the availability of nutrients. Equation (1) differs from the ones used in several *in situ* approaches for the study of crop productivity, where an explicit parameter $fmax$ defines the maximum flow of photon that the plant is able to process. We disregarded this approach given that light is unlike to be the limiting factor in wild plants and we didn't find applications in the remote sensing literature. We tested three different proxies of $fAPAR$, extracted from Sentinel2 level1 data downloaded from the Copernicus Data Hub: modified soil adjusted vegetation index 2 (MSAVI2, Qi et al. (1994); Henrich et al. (2012)), Modified Chlorophyll abortion ration index 2 (MCARI2, Haboudane et al. (2004)) and FAPAR estimated using the sen2core neural network application (Main-Knorn et al. (2017)). Notice that we use a different letter case to distinguish the variable $fAPAR$ from the sen2core estimator FAPAR. The Sentinel2 topographic correction and the combined

https://doi.org/10.5194/egusphere-2023-2824
Preprint. Discussion started: 23 January 2024

system of snow and cloud filtering (Richiardi et al., 2021) were performed using the same mosaic DTM also used for shade estimation. In total, 394 images from the beginning of 2017 to the end of 2020 were stacked. Then, using a cloud filtering pipeline, pixels identified as cloud were marked as "data not available", while snow pixels were marked as "zero", given that $fAPAR$ is null under the snow cover. The five Nivolet time-series features, overlapping the five case study plots, were extracted and signal-cleaned following two different procedures: i) Savigtzy-Golay filtering (Chen et al., 2004) as implemented in the python module *scipy* using a window of 17 observations and a quadratic polynomial; ii) PPresil Harmonic based modelling (Vicario et al., 2019) using yearly, biannual and four-month harmonics. Starting from equation (1), we expanded APAR and modelled LUE as a summation of measured predictors:

$$GPP = a1 + a2(PAR \cdot fAPAR) \cdot \sum_i a3i \cdot Anc_i \tag{2}$$

where Anc_i are the predictors of LUE. The presence of an intercept in the equation allows to manage systematic bias in the scaling of the variables, but obviously does not allow to predict zero productivity in absence of light. The list of candidate predictors for primary productivity tested in this work is detailed in table 1. We explored 4 predictors of PAR, as summarised in figure 1: 3 proxies from ERA5 (ssrd, Radiance_Mod, ssrdXSVF) and 1 proxy from MODIS data.

The ERA5 reanalysis model from the Copernicus Climate Change Service allows to distinguish between direct and indirect light and has a temporal resolution of 1 hour. The spatial resolution is limited to a quarter of degree that can be interpolated to a hundred of degrees; for the study site, this means about 800 m along longitude and 1000 m along latitude. From the ERA5 data we extracted 3 proxies of incident PAR: Surface Solar Radiation Downwards (acronym: ssrd), the ssrd corrected by the Sky View factor (ssrdXSVF), the sum of direct radiation (fdir) corrected by terrain effect (propdir) and the indirect radiation corrected by the Sky View factor (Radiance_Mod). To estimate terrain effect, the R package *insol* was used (Corripio, 2021). The package estimates both self and cast shade using a Digital Terrain Model (DTM) and sun position. We produced a mosaic of Piedmont Regional DTM (10m resolution, epsg:32632), Aosta valley regional DTM (2m resolution, epsg:4230) and Copernicus EU DTM ver 1.1 (25m resolution, epsg:3035) for the full frame of Sentinel2, overlapping Nivolet valley and using a final resolution of 6.6 m and the projection epsg:32632. Re-projection and mosaic were performed with *gdal* utilities (GDAL/OGR contributors, 2023). The Sky View factor (SVF) varies from zero on the bottom of narrow gorges, to 1 in flatlands, and it was estimated by the *r.skyview* routine of GRASS (GRASS Development Team, 2022) evaluating the same mosaic DTM.

The fourth selected proxy to the incident PAR was MCD18A2061, the PAR product estimated from MODIS data by NASA. This product is available from 2000 to 2022 at 1km resolution using albedo and land cover information from Wang et al. (2020). Because *in situ* measurements were taken in different times of the day, we used the estimation projected every 3 hours and not the instantaneous estimate done at time of satellite passage (10:30 GMT). We did not apply further corrections for terrain effect because the product, at least partially, already includes it through the albedo.

The set of candidate Anc_i variables used to express LUE (see equation 2) included several ones from the ERA5 model using the same resolution and interpolation method employed for the radiation data: surface air pressure (sp), air and dew temperature at 2 m (t2m and d2m), and soil temperature and water content within the upper 7 cm (stl1, swl1). From t2m and d2m we estimated relative humidity as the ratio of the vapour pressures at actual and dew temperature. Vapour pressure was

https://doi.org/10.5194/egusphere-2023-2824
Preprint. Discussion started: 23 January 2024

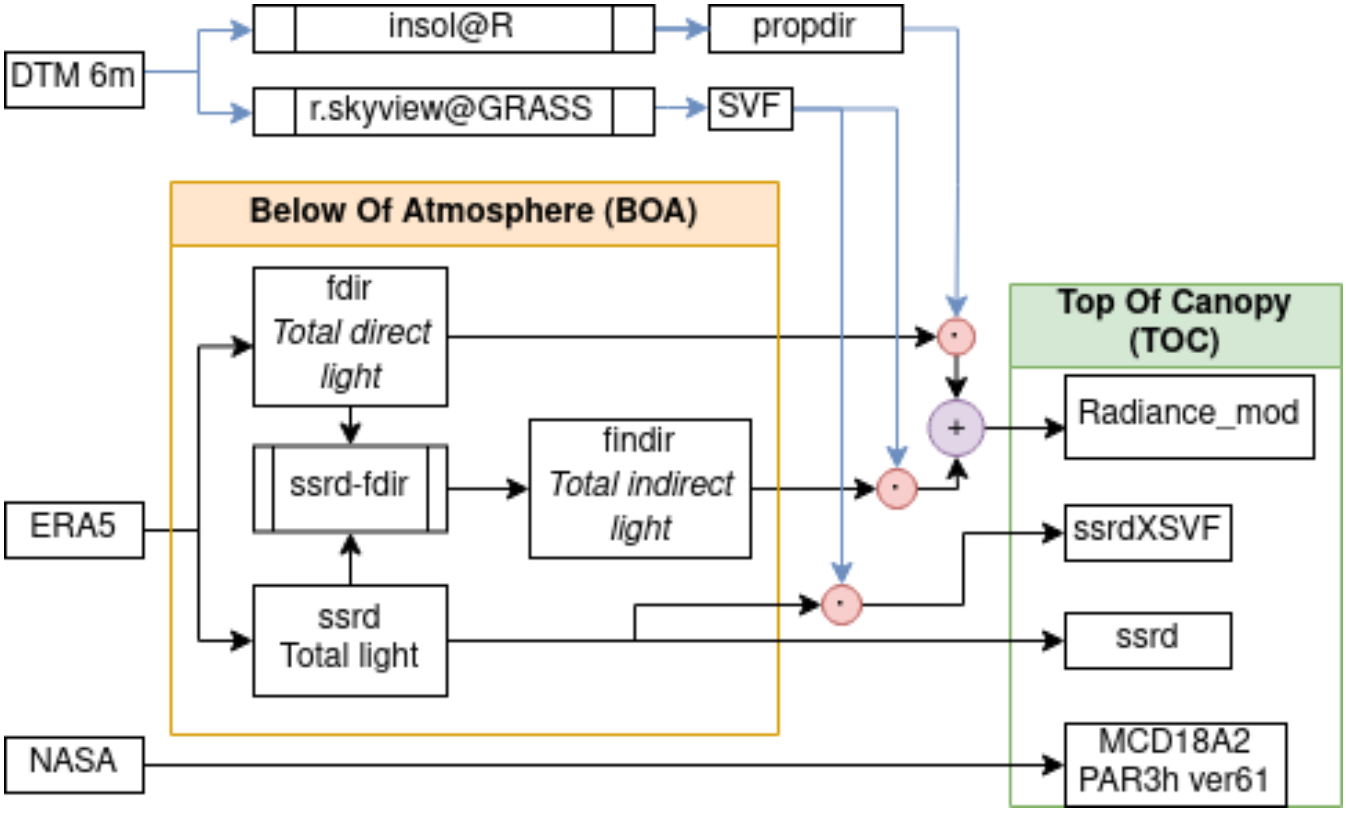

Figure 1. Diagram of the 4 PAR_{inc} proxy derivations, implemented using NASA product and the estimate of direct and indirect light from ERA5, combined with propdir and SVF from DTM information.

calculated from temperature using the Buck equation (Junzeng et al., 2012):

$$V_p(T) = 0.61121e^{(18.678-\frac{T}{234.5})(\frac{T}{257.14+T})} \quad (3)$$

To align these variables with the timing of the *in situ* measures, we implemented a weighted mean approach in which weights were proportional to the overlap between remote variable and the time period of the *in situ* measure.

For the remote sensing estimates of LUE, the time series of the Photochemical Reflectance Index (PRI) was extracted from the MODIS dataset using Google Earth engine (Gorelick et al., 2017). The PRI was calculated when both bands showed a zero quality flag, the sensor position was farther than 15 degrees from nadir and the difference in azimuth between the sensor and the sun was more than 60 degrees Middleton et al. (2016). Similarly to Sentinel-2 time series, also the MODIS time series was cleaned using the same two procedures, with the only difference being adding the bimonthly harmonic to take into account the sharp increase of PRI at the start of the productive season. In fact, using smaller harmonic allows the model to follow faster changes (Geerken, 2009). After a preliminary exploration of the data in which the complementarity between MSAVI2 and MCARI2 information was observed, we added the ratio of MCARI2 over MSAVI2 as one of the candidate predictors in the

https://doi.org/10.5194/egusphere-2023-2824
Preprint. Discussion started: 23 January 2024

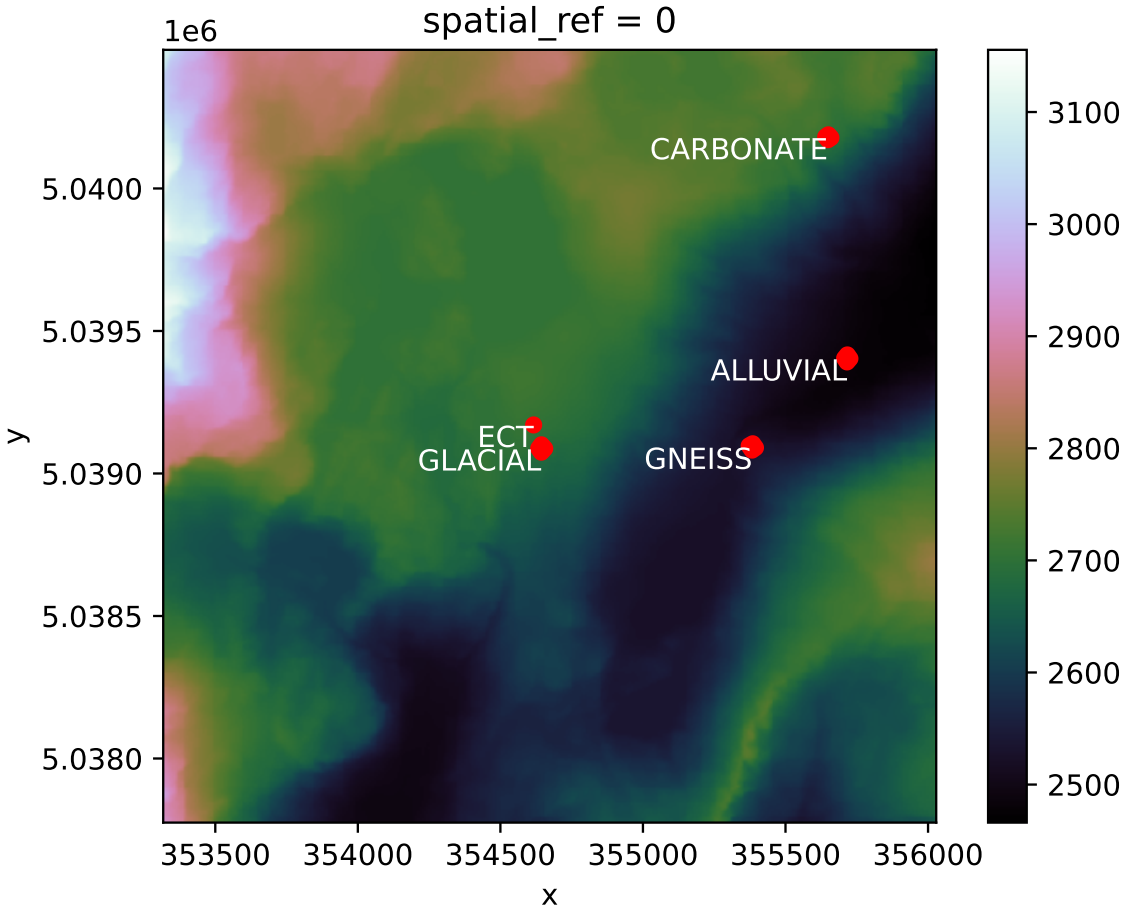

Figure 2. Mosaic Digital Terrain Model (DTM) image of the Nivolet Valley with the location of the sampling sites identified by red points. The image is projected with UTM 32N, allowing to read the distances in meters after multiplying the tick value by the coefficient at the end of each axis (10^6 and 10^5 respectively for N and E coordinates).

models. This ratio allows to estimate the concentration of chlorophyll with respect to the rest of the leaves pigment pool. We noticed that using it as an estimator of LUE further improved the model.

2.3 Model Selection

In order to build a model that is robust to extrapolation, we used a cross-validation approach for its selection, where the model is fit only on a portion of the data and tested on the remaining portion (Berrar, 2019). To take into account the structure of the dataset (different sites and different years) a by block strategy was preferred (Roberts et al., 2017). Four different types of

https://doi.org/10.5194/egusphere-2023-2824
Preprint. Discussion started: 23 January 2024

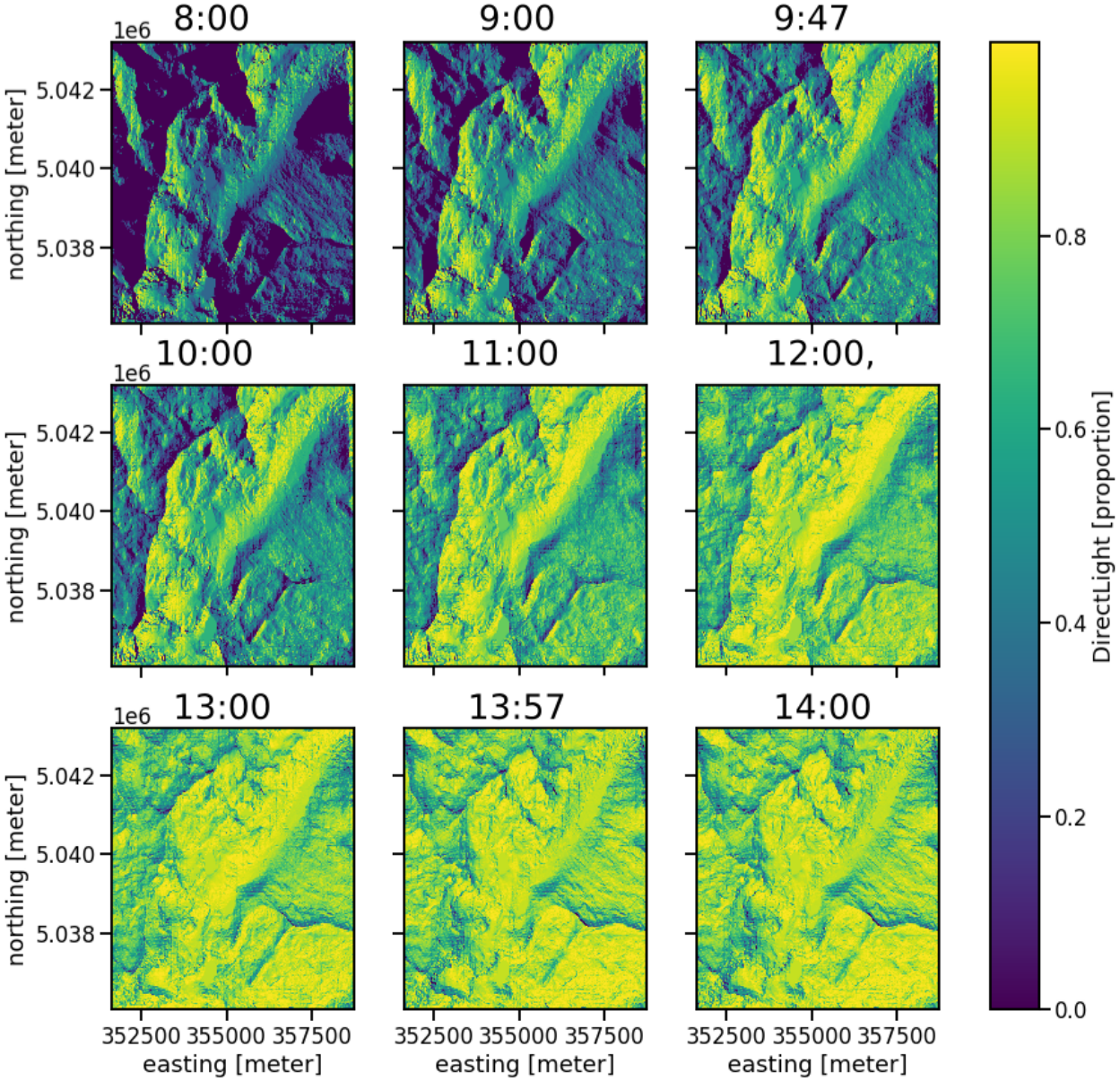

Figure 3. Estimated time series of the PAR fraction that actually hits the surface as direct light at the bottom of the atmosphere in July 12th 2017 using UTC time. Same DTM as Fig. 2.

https://doi.org/10.5194/egusphere-2023-2824
Preprint. Discussion started: 23 January 2024

Use	Variable	*in situ*	Sat. RS	ERA5	Spatial Res.	Time Res.
	PAR	Radiance	-	ssrd	800m†	1h
|	PAR	Radiance	-	Radiance_Mod	800m†	1h
	PAR	Radiance	-	ssrdXSVF	800m†	1h
	PAR	Radiance	$PAR3h_{MCD18A2}$	-	1km	3h
	$fAPAR$	-	$MSAVI2_{S2}$	-	10m	2g‡
|	$fAPAR$	-	$MCARI2_{S2}$	-	10m	2g‡
	$fAPAR$	-	$FAPAR_{S2}$	-	10m	2g‡
	Zea/Violaxant.	-	PRI_{MODIS}	-	1km	1g‡
	Chl./All Pigmt.	-	$PropVI_{s2}$		10m	2g‡
	Air Pressure	Pressure	-	sp	800m†	1h
+	Relative Humidity	AirMoist	-	RH	800m†	1h
	Soil Temperature	SoilTemp	-	stl1	800m†	1h
	Air Temperature	AirTemp	-	t2m	800m†	1h
	Volumetric Water Content	VWC	-	swvl1	800m†	1h
	Vapour Pressure Deficit	VPD	-	vpd	800m†	1h

Table 1. Explored predictors, their sources and resolutions. The first column indicates the use in the *formulae*: " | " when different variables are used alternatively in the same formula, "+" when they can be used simultaneously. Subscripts report details about the data source. Under the mid line are listed variables that were tested as candidate predictors of Light Use Efficiency (LUE). Variables with † are interpolated, original model resolution is $0.25°$ (25km). Variables with ‡ are instantaneous measurements spaced as indicated in "Time Res." column. The remaining values are integrated over the time span indicated in the "Time Res." column. All the *in situ* measurements were performed simultaneously with the flux measurements, and the reported values are the mean values across the 20 individual points taken at each plot during the 1-2h sampling time.

https://doi.org/10.5194/egusphere-2023-2824
Preprint. Discussion started: 23 January 2024

cross-validation were performed: i) the *"leave one [observation] out"* procedure (LOO), which tackled the prediction ability on a single unseen observation, to gauge the possibility to cope with anomalies; ii) the *"leave one location out"* and *"leave one year out"* procedures (LOPO e LOYO, which respectively evaluated the spatial and temporal extrapolations); iii) the *"leave one combination of plot and year out"* procedure (LOPYO), which finally evaluated the model against combined space and time extrapolations. Under each of these procedures, we used the explained variance (R^2) as optimality indicator, and we merged these four values using a geometric mean to obtain a single explained variance indicator, called Av.LOO, as shown in the equation below:

$$Av.Loo = \begin{cases} CV = (LOO, LOPO, LOYO, LOPYO) \\ \prod_{i \in CV}^{n} (R_i^2)^{\frac{1}{n}} \end{cases} \quad (4)$$

where *n* is the number of cross validation procedures over which the geometric mean is calculated.

To explore the marginal contribution of each plot or year to optimality score of the different models, we implemented a strategy similar to the weighted Akaike criterion (Burnham and Anderson, 2001) based on the integrated cross-validation indicator $Av.LOO$. As this indicator is indeed correlated with the likelihood of the model and so could be scaled to AIC value making twice the negative logarithm of $Av.LOO$. On this transformed value we applied the weighted Akaike procedure:

$$\begin{aligned} M &= (m_1, ..., m_i, ...m_N) \\ pAIC_i &= 2\log(Avv.LOO_i) + 2k_i \\ \Delta_i &= pAIC_i - pAIC_{bestmodel} \\ w_i &= \frac{e^{-\frac{\Delta_i}{2}}}{\sum_{r=1}^{N} e^{-\frac{\Delta_r}{2}}} \\ I_p &= \{i | p \in m_i\} \\ w_p &= \sum_{i \in I} w_i \end{aligned} \quad (5)$$

In the equation 5, assuming M the set of evaluated models, and pAIC the proxy AIC calculated based on $Av.LOO$ and k the number of parameter used, we can define a weight w_i for i^{th} model and summing all weights of models in which a given parameter p appears we can calculated its overall weight across all models called w_p.

3 Results

3.1 Measurements

Since meteo-climatic measurements are missing in some of the *in situ* sampling campaigns, a subset composed of 73 complete observations (fluxes and meteo-climatic data) was extracted from the full dataset of 85 observations (Table 2). This subset of the dataset was used in the modelling approach based only on *in situ* data. The full set of 85 flux observations was instead used to develop the model based on ancillary variables derived from remote sensing.

https://doi.org/10.5194/egusphere-2023-2824
Preprint. Discussion started: 23 January 2024

Year Plot	2017	2018	2019	2020
ALLUVIAL	2/3	2/4	2/4	5
CARBONATE	2/3	5/6	4/5	6
GLACIAL	3/4	6	5/6	6
GNEISS	4	5	4/6	6
ECT	-	-	-	6

Table 2. Number of observations of GPP and ancillary data across different plots and years at Nivolet Plain. The number before the slash indicates the subset of observations with no missing ancillary data, while the number after the slash indicates the total number of observations.

To estimate the correspondence between the ERA5 and NASA ancillary data with *in situ* measurements of meteo-climatic variables, we performed a simple regression and we used the same cross-validation procedures as explained above for the GPP model. As shown in table 3, only atmospheric pressure, after altitudinal correction, is satisfactorily estimated by ERA5 in the Nivolet area. The other variables showed an explained variance around 50% or lower. Focusing on PAR estimators, the best result, obtained by Radiance_Mod, did not reach 50% of explained variance, but the Av.LOO score showed that the need to evaluate the systematic underestimation of incident shortwave radiation undermined the robustness of the estimate. For this reason, ssrdXSVF had a better Av.LOO score. The good Av.LOO score of this model could be due to the fact that the shoots, thanks to their known negative gravitropism, counterbalanced the effect of slope on the average leaves exposition (Bastien et al., 2013; Firn et al., 1999; Zhang et al., 2019). The MCD18A2_PAR3h had the lowest R^2 among radiance products, whereas the instantaneous product tested only on the observations within an hour of the time of passage of the MODIS satellite gave much better results, but it applied only to few observations and for this reason was not shown here.

3.2 Marginal parameters contribution

To identify the marginal parameters contribution of each *in situ* and spectral predictor we used a correlation matrix (see Fig. 4). For simplicity we used only Radiance_Mod as remote estimator of Radiance, given that it is the best among the 4 tested ones (Table 3). The spectral indices form a compact cluster where all members were significantly correlated with $P< 0.005$ and all of them but PRI were significantly correlated with GPP. The remote radiance and temperature and humidity of soil and air formed a cluster, as well as the spectral indices. On the contrary, between *in situ* data this cluster broke in two pieces with air temperature as only link among the two. Using *in situ* data, the only significant correlation between this two cluster was PropVI that significantly correlated with Relative Humidity and soil water content. Using remote data, the situation was quite different with Radiance, Air and Soil Temperature that significantly correlated with all spectral indices. It is quite likely that all these extra correlations in the remote sensing dataset were spurious because all variables were extracted from the same model.

https://doi.org/10.5194/egusphere-2023-2824
Preprint. Discussion started: 23 January 2024

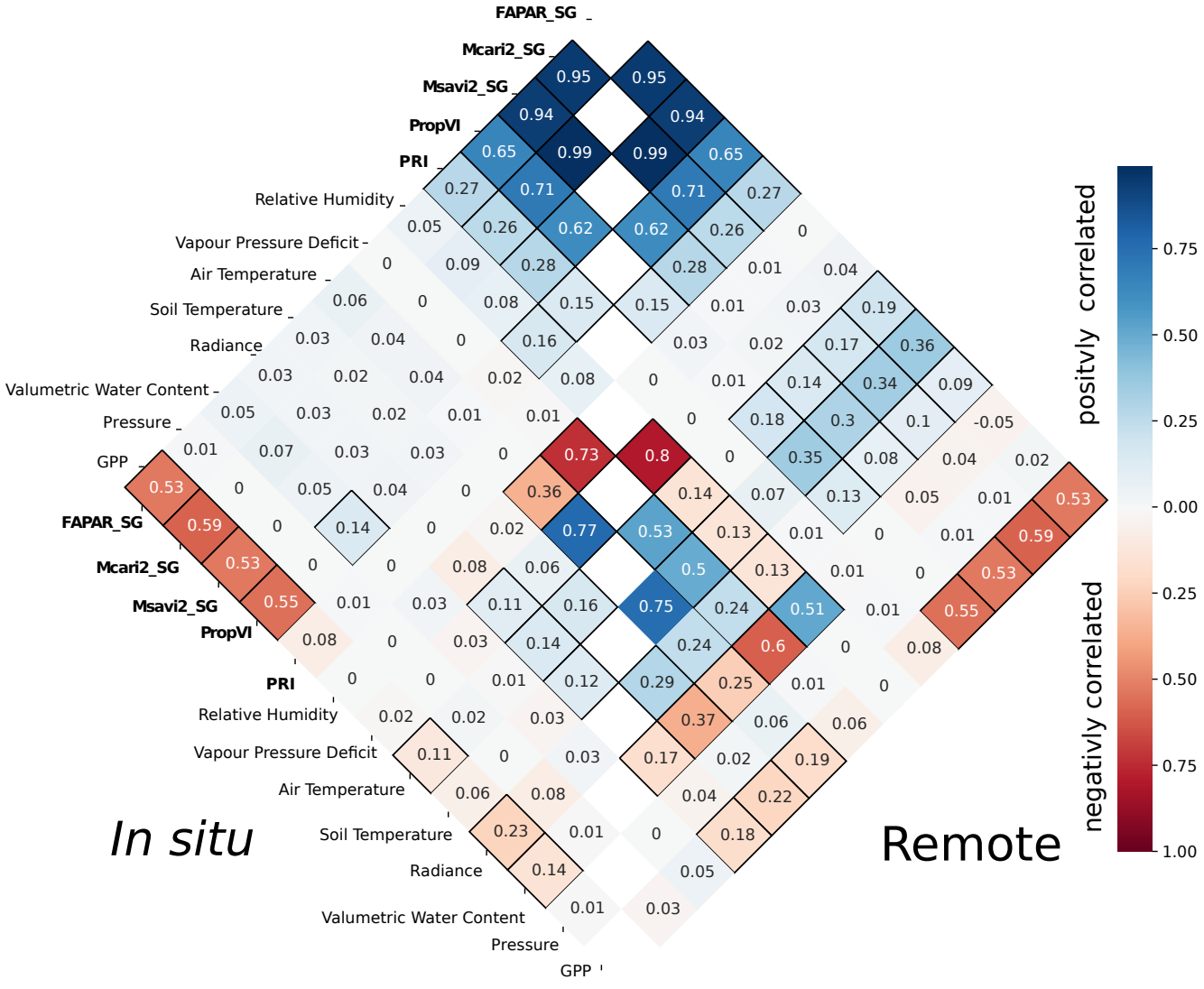

Figure 4. Square of the correlation coefficients between all *in situ* and spectral predictors and the *in situ* estimated GPP using the 73-observations dataset. On the left, the correlation among *in situ* measures and spectral indexes (in bold), while on the right the same spectral indexes correlate with ERA5 estimates of the same variables. Hue indicates the sign of the correlation, boxed cells indicate significant correlations at 0.005 level and white digits indicate correlation values higher than 0.5.

https://doi.org/10.5194/egusphere-2023-2824
Preprint. Discussion started: 23 January 2024

Remote	*in situ*	R^2	Av.LOO	MeanBias
ssrdXSVF	Radiance	0.43	0.39	0.35
ssrd		0.38	0.33	0.20
Radiance_Mod		0.49	0.38	0.37
MCD18A2_PAR3h		0.18	1.0×10^{-4}	0.19
sp	AirPressure	0.83	0.81	−0.00
RH	AirMoist	0.53	0.49	−0.10
stl1	SoilTemp	0.23	4.18×10^{-4}	−0.10
t2m	AirTemp	0.35	0.29	−0.04
swvl1	SoilMoist	0.00	1.00×10^{-4}	0.11
vpd	VPD	0.34	0.28	0.13

Table 3. Evaluation of the relationships between estimators based on remote sensing and *in situ* ones.

3.3 Best Models Results

Table 4 reports the best models and their scores. The linear model informed by *in situ* data outperformed MOD17 increasing the Av.LOO by 0.10. Using the same 73-observation dataset and only remote sensing data, this difference decreased to 0.04. Using the full 85-observation dataset, the estimates based on remote sensing ancillary data outperformed MOD17 by 0.09.

Several combinations of parameters using only remote sensing data produced higher Av.LOO score than MOD17 and their relative importance could be inferred using the weighted Akaike procedure (see panel d in Fig. 6). The calculation of the Akaike Information Criterion (AIC)(Fig. 6) was performed on all models that showed a value of Av.LOO better than the one obtained for MOD17, previously divided into 3 groups: "RS", including models fitted on the 85 observations set using only remote predictor; "RS73" using the same predictors of the group "RS" but with the dataset composed of the 73 complete observations; and finally the group "Local" formed by models that use the 73 observations dataset and only *in situ* predictors. The models of the groups "RS" and "RS73" performed better using ssrd as PAR predictor. For $fAPAR$ estimate, all 3 groups of models had higher score using Msavi2, although both groups "RS" and "Local" presented a small difference with other $fPAR$ estimators. When the intercept ("a1" in the equation 2) was removed, the model score dropped and, in the case of RS73, none of them performed better than MOD17 (see panel b in figure 6). The ancillary parameter PropVI was present in almost all models that perform better than MOD17, followed by PRI that has quite a high AIC value in the RS group. For the other ancillary variables there was less consensus across datasets and models. For example, VPD was the third ancillary variable preferred for remote sensing ancillary data and 85 observations, but was the fourth in the 73 observation, and became the sixth if we used local measurements of ancillary data (see panel c in figure 6). These diverse roles of the climate variables across remote and local estimates is quite evident also looking at figure 4.

https://doi.org/10.5194/egusphere-2023-2824
Preprint. Discussion started: 23 January 2024

Source	*in situ*			S2+ERA5+MODIS	
Obs.	73			85	
VI	Mcari2	FAPAR		Mcari2	
Ancillary	PropVI +PRI +AirMoist	vpd+ProVI	MOD17	PropVI +PRI +vpd	MOD17
PAR	Radiance	ssrd		ssrd	
R^2	0.81	0.73	0.68	0.76	0.64
LOO	0.76	0.69	0.67	0.71	0.62
LOPO	0.75	0.70	0.61	0.71	0.53
LOYO	0.73	0.67	0.66	0.65	0.60
LOPYO	0.77	0.70	0.66	0.68	0.61
Av.LOO	0.75	0.69	0.65	0.68	0.59

Table 4. Best models with and without using *in situ* data compared to results of locally calibrated MOD17 model. On columns 2,3,4 models are fitted using the smaller, complete dataset, were all *in situ* variables are available, while on the right (columns 5 and 6) the models are fitted to the 85-observation dataset. R^2 is the explained variance, and the rows below it indicate the different cross-validation procedures as detailed in the text (Section 2.3)

4 Discussion and Conclusions

The proposed approach for remote sensing estimation of GPP in Alpine grasslands led to a significant, albeit small, improvement compared to MOD17. The Av.LOO score for the "remote" model compared negatively with the one obtained for the *in situ* fed model, and it did not reach the values near 80-90% obtained for *in situ* ancillary data (see table 4). The problem does not seem to be related to the lack of data, given that using the individual point measurements, which increased the sample size from 85 to 492, did not change the quality of the estimation and the relative comparison between models.

Looking at the different components of Av.LOO in the RS85 model (Table 4), it is clear that much of the complexity was due to the interannual variability, in agreement with Lenzi et al. (2023). On the other hand, plot-to-plot variability was low, suggesting the possibility of spatially extrapolating the model to other measurement sites or even different valleys, provided we consider grassland environments. Further work should thus explore the spatial portability of the model developed here to different high-altitude grassland environments in the Alps.

An advantage of this model is that the selected predictors are easily computed at large scale and only a reasonable number of calibration points was required to fit the model for different kinds of Alpine grasslands. In previous works concerning the

https://doi.org/10.5194/egusphere-2023-2824
Preprint. Discussion started: 23 January 2024

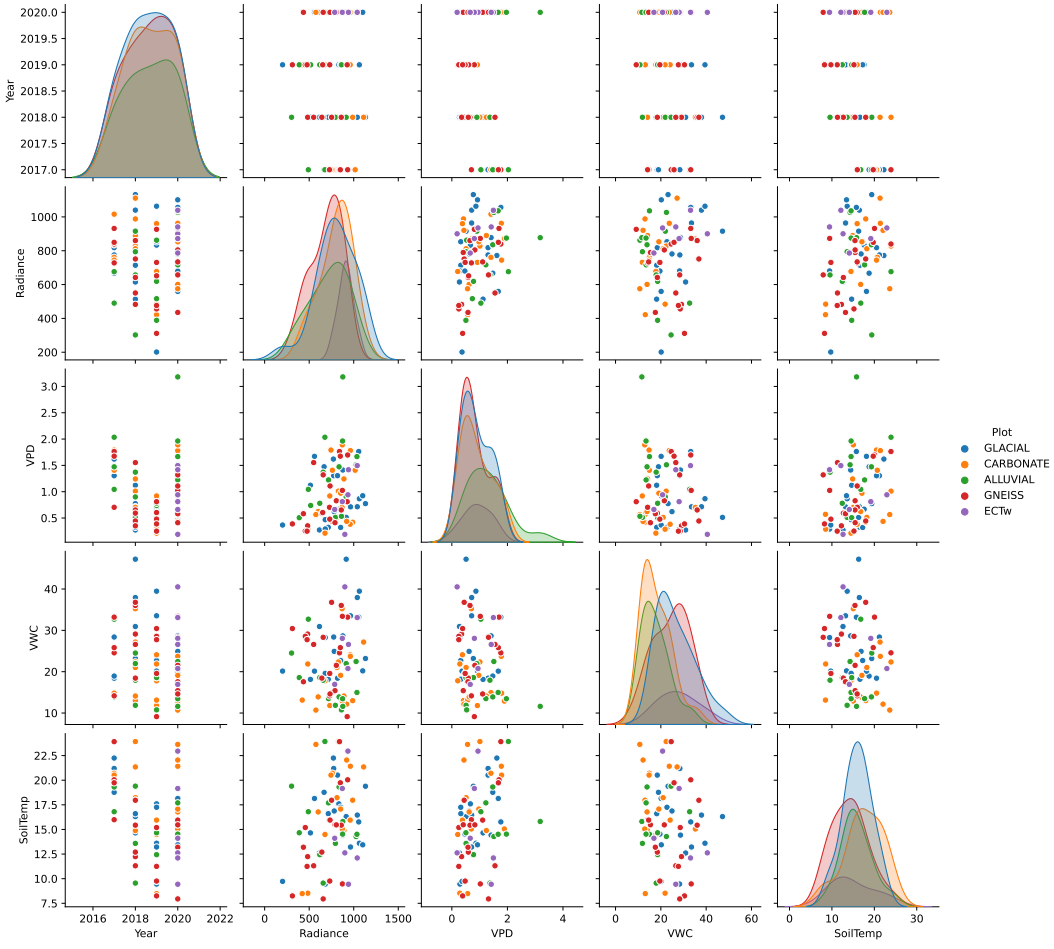

Figure 5. Pair plots of the Radiance, VPD, VWC and SoilTemp across the Nivolet plots. The ECT plot was excluded for simplicity.

study of lowland grasslands (Wang et al. (2017); Ferreira et al. (2021)), MOD17 has been shown to produce only $R^2 < 0.7$. In this work, we proposed alternatives to MOD17 and tested the performance of the alternative models when using only remote sensing products as climatic and environmental drivers. The results confirmed the possibility to set up empirical local models that capture the site-specific carbon fixation dynamics using only remote-sensing estimates and open repository data as drivers.

https://doi.org/10.5194/egusphere-2023-2824
Preprint. Discussion started: 23 January 2024

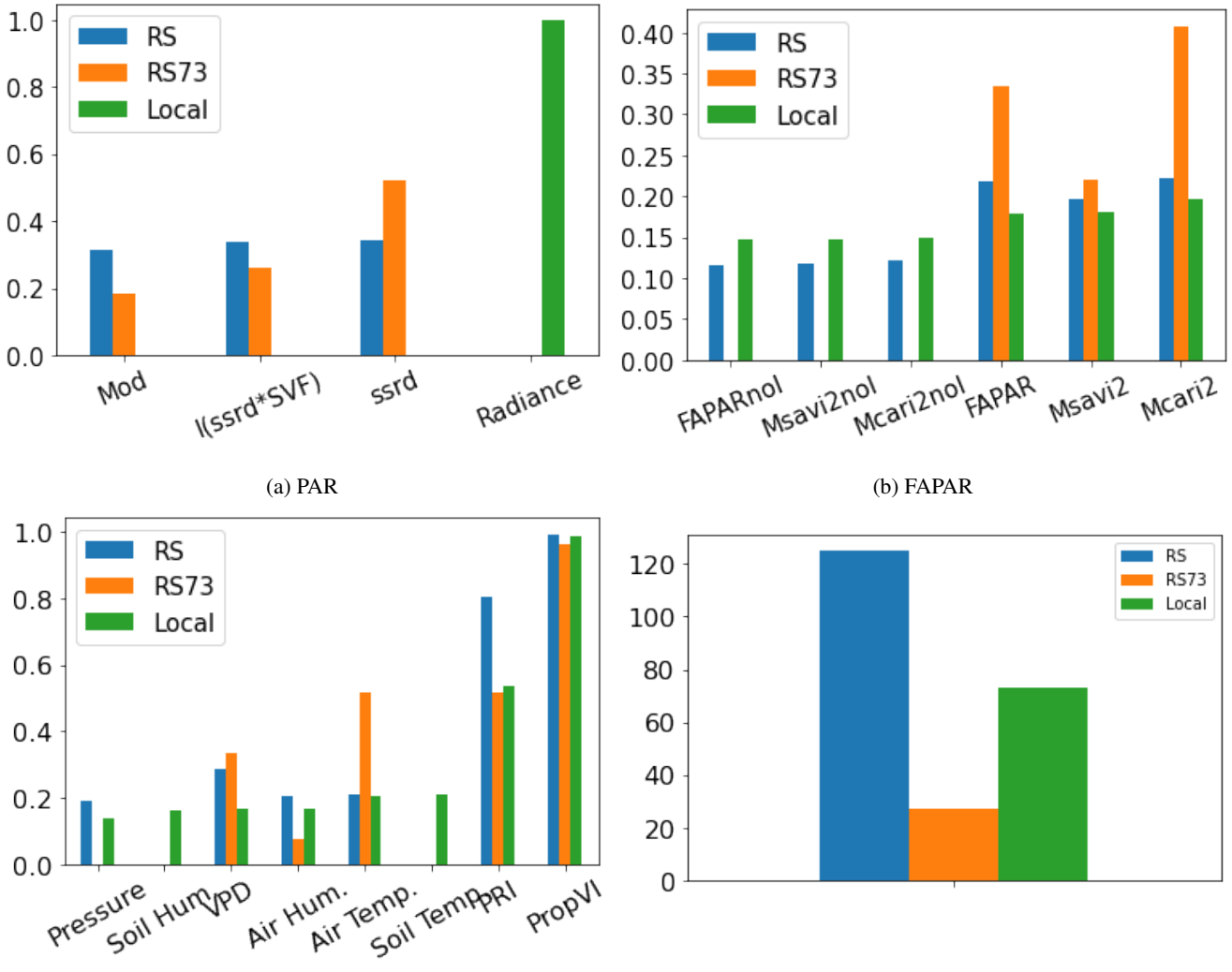

(a) PAR

(b) FAPAR

(c) Ancillary

(d) Number of Models

Figure 6. Weighted cross-validation score contribution of the parameters. Panels a), b) and c) describe contribution of alternative choices for PAR, FAPAR and Ancillary, respectively, to the explained variance of the models "RS", "RS73" and "local". The RS set includes only remotely inferred parameters over the 85 observations dataset, while 'Local' refers to only *in situ* measured parameters over the 73 observations dataset, finally RS73 refers to all remotely inferred parameters using the same dataset of *in situ* data.

https://doi.org/10.5194/egusphere-2023-2824
Preprint. Discussion started: 23 January 2024

References

Balsamo, G., Agusti-Panareda, A., Albergel, C., Arduini, G., Beljaars, A., Bidlot, J., Bousserez, N., Boussetta, S., Brown, A., Buizza, R., Buontempo, C., Chevallier, F., Choulga, M., Cloke, H., Cronin, M. F., Dahoui, M., Rosnay, P. D., Dirmeyer, P. A., Drusch, M., Dutra, E., Ek, M. B., Gentine, P., Hewitt, H., Keeley, S. P., Kerr, Y., Kumar, S., Lupu, C., Mahfouf, J. F., McNorton, J., Mecklenburg, S., Mogensen, K., Muñoz-Sabater, J., Orth, R., Rabier, F., Reichle, R., Ruston, B., Pappenberger, F., Sandu, I., Seneviratne, S. I., Tietsche, S., Trigo, I. F., Uijlenhoet, R., Wedi, N., Woolway, R. I., and Zeng, X.: Satellite and in situ observations for advancing global earth surface modelling: A review, https://doi.org/10.3390/rs10122038, 2018.

Baneschi, I., Raco, B., Magnani, M., Giamberini, M., Lelli, M., Mosca, P., Provenzale, A., Coppo, L., and Guidi, M.: Non-steady-state closed dynamic chamber to measure soil CO2 respiration: A protocol to reduce uncertainty, Frontiers in Environmental Science, 10, https://doi.org/10.3389/fenvs.2022.1048948, 2023.

Bastien, R., Bohr, T., Moulia, B., and Douady, S.: Unifying model of shoot gravitropism reveals proprioception as a central feature of posture control in plants, Proceedings of the National Academy of Sciences of the United States of America, 110, 755–760, https://doi.org/10.1073/pnas.1214301109, 2013.

Berrar, D.: Cross-Validation, in: Encyclopedia of Bioinformatics and Computational Biology, edited by Ranganathan, S., Gribskov, M., Nakai, K., and Schönbach, C., pp. 542–545, Academic Press, Oxford, https://doi.org/https://doi.org/10.1016/B978-0-12-809633-8.20349-X, 2019.

Buchhorn, M., Smets, B., Bertels, L., De Roo, B., Lesiv, M., Tsendbazar, N.-E., Herold, M., and Fritz, S.: Copernicus global land service: Land cover 100m: collection 3: epoch 2019: Globe, Version V3. 0.1, 2020.

Burnham, K. P. and Anderson, D. R.: Kullback-Leibler information as a basis for strong inference in ecological studies, Wildlife Research, 28, 111–119, https://doi.org/10.1071/WR99107, 2001.

Chen, J., Jönsson, P., Tamura, M., Gu, Z., Matsushita, B., and Eklundh, L.: A simple method for reconstructing a high-quality NDVI time-series data set based on the Savitzky-Golay filter, Remote Sensing of Environment, 91, 332–344, https://doi.org/10.1016/j.rse.2004.03.014, 2004.

Corripio, J. G.: Insol: an R packages, https://cran.r-project.org/src/contrib/Archive/insol/, accessed 2023-08-20, 2021.

Danna, C., Poggio, L., Smeriglio, A., Mariotti, M., and Cornara, L.: Ethnomedicinal and ethnobotanical survey in the Aosta valley side of the Gran Paradiso National Park (Western Alps, Italy), Plants, 11, 170, 2022.

de Paula, M. D., Giménez, M. G., Niamir, A., Thurner, M., and Hickler, T.: Combining European Earth Observation products with Dynamic Global Vegetation Models for estimating Essential Biodiversity Variables, International Journal of Digital Earth, 13, https://doi.org/10.1080/17538947.2019.1597187, 2020.

Ferreira, R. R., Santos E Silva, C. M., Bezerra, B., Mendes, K. R., Mutti, P., Campos, S., Marques, T. V., P. Oliveira, C., Gonçalves, W., Espinoza, N., Difante, G., and Urbano, S. A.: A brief evaluation of the MOD17A2H product over a pasture in northeast Brazil, Remote Sensing Letters, 12, 50–57, https://doi.org/10.1080/2150704X.2021.1875144, 2021.

Filippa, G., Cremonese, E., Galvagno, M., Bayle, A., Choler, P., Bassignana, M., Piccot, A., Poggio, L., Oddi, L., Gascoin, S., et al.: On the distribution and productivity of mountain grasslands in the Gran Paradiso National Park, NW Italy: A remote sensing approach, International Journal of Applied Earth Observation and Geoinformation, 108, 102 718, 2022.

Firn, R., Wagstaff, C., and Digby, J.: The ups and downs of gravitropism, Trends in Plant Science, 4, 252, https://doi.org/10.1016/S1360-1385(99)01434-X, 1999.

https://doi.org/10.5194/egusphere-2023-2824
Preprint. Discussion started: 23 January 2024

Friedlingstein, P., O'sullivan, M., Jones, M. W., Andrew, R. M., Gregor, L., Hauck, J., Le Quéré, C., Luijkx, I. T., Olsen, A., Peters, G. P., et al.: Global carbon budget 2022, Earth System Science Data Discussions, 2022, 1–159, 2022.

Gamon, J. A., Peñuelas, J., and Field, C. B.: A narrow-waveband spectral index that tracks diurnal changes in photosynthetic efficiency, Remote Sensing of Environment, 41, 35–44, https://doi.org/10.1016/0034-4257(92)90059-S, 1992.

GDAL/OGR contributors: GDAL/OGR Geospatial Data Abstraction software Library, Open Source Geospatial Foundation, https://doi.org/10.5281/zenodo.5884351, 2023.

Geerken, R. A.: An algorithm to classify and monitor seasonal variations in vegetation phenologies and their inter-annual change, ISPRS Journal of Photogrammetry and Remote Sensing, 64, 422–431, https://doi.org/10.1016/j.isprsjprs.2009.03.001, 2009.

Gorelick, N., Hancher, M., Dixon, M., Ilyushchenko, S., Thau, D., and Moore, R.: Google Earth Engine: Planetary-scale geospatial analysis for everyone, Remote Sensing of Environment, 202, 18–27, https://doi.org/10.1016/j.rse.2017.06.031, 2017.

GRASS Development Team: Geographic Resources Analysis Support System (GRASS GIS) Software, Version 8.2, Open Source Geospatial Foundation, https://grass.osgeo.org, 2022.

Haboudane, D., Miller, J. R., Pattey, E., Zarco-Tejada, P. J., and Strachan, I. B.: Hyperspectral vegetation indices and novel algorithms for predicting green LAI of crop canopies: Modeling and validation in the context of precision agriculture, Remote Sensing of Environment, 90, 337–352, https://doi.org/10.1016/J.RSE.2003.12.013, 2004.

Henrich, V., Krauss, G., Götze, C., and Sandow, C.: Index Database, https://www.indexdatabase.de/db/i-single.php?id=44, accessed 2023-08-20, 2012.

Junzeng, X., Qi, W., Shizhang, P., and Yanmei, Y.: Error of Saturation Vapor Pressure Calculated by Different Formulas and Its Effect on Calculation of Reference Evapotranspiration in High Latitude Cold Region, Procedia Engineering, 28, 43–48, https://doi.org/10.1016/j.proeng.2012.01.680, 2012.

Lehmann, A., Masò, J., Nativi, S., and Giuliani, G.: Towards integrated essential variables for sustainability, https://doi.org/10.1080/17538947.2019.1636490, 2020.

Lenzi, S., Magnani, M., Baneschi, I., Giamberini, M., Raco, B., Vivaldo, G., and Provenzale, A.: Spatial and temporal variability of carbon dioxide fluxes in the Alpine Critical Zone: The case of the Nivolet Plain, Gran Paradiso National Park, Italy, PLOS ONE, 18, e0286 268, https://doi.org/10.1371/journal.pone.0286268, 2023.

Li, Y., Dong, S., Liu, S., Su, X., Wang, X., Zhang, Y., Zhao, Z., Gao, X., Li, S., and Tang, L.: Relationships between plant diversity and biomass production of alpine grasslands are dependent on the spatial scale and the dimension of biodiversity, Ecological Engineering, 127, 375–382, https://doi.org/10.1016/j.ecoleng.2018.12.015, 2019.

Magnani, M., Baneschi, I., Giamberini, M., Mosca, P., Raco, B., and Provenzale, A.: Drivers of carbon fluxes in Alpine tundra: a comparison of three empirical model approaches, Science of the Total Environment, 732, 139 139, https://doi.org/10.1016/j.scitotenv.2020.139139, 2020.

Main-Knorn, M., Pflug, B., Louis, J., Debaecker, V., Müller-Wilm, U., and Gascon, F.: Sen2Cor for Sentinel-2, in: Image and Signal Processing for Remote Sensing XXIII, edited by Bruzzone, L., Bovolo, F., and Benediktsson, J. A., p. 3, SPIE, https://doi.org/10.1117/12.2278218, 2017.

Mainetti, A., D'Amico, M., Probo, M., Quaglia, E., Ravetto Enri, S., Celi, L., and Lonati, M.: Successional herbaceous species affect soil processes in a high-elevation alpine proglacial chronosequence, Frontiers in Environmental Science, 8, 615 499, 2021.

https://doi.org/10.5194/egusphere-2023-2824
Preprint. Discussion started: 23 January 2024

Middleton, E. M., Huemmrich, K. F., Landis, D. R., Black, T. A., Barr, A. G., and McCaughey, J. H.: Photosynthetic efficiency of northern forest ecosystems using a MODIS-derived Photochemical Reflectance Index (PRI), Remote Sensing of Environment, 187, 345–366, https://doi.org/10.1016/j.rse.2016.10.021, 2016.

Piana, F., Fioraso, G., Irace, A., Mosca, P., D'atri, A., Barale, L., Falletti, P., Monegato, G., Morelli, M., Tallone, S., et al.: Geology of Piemonte region (NW Italy, Alps–Apennines interference zone), Journal of Maps, 13, 395–405, 2017.

Porcar-Castell, A., Tyystjärvi, E., Atherton, J., Van Der Tol, C., Flexas, J., Pfündel, E. E., Moreno, J., Frankenberg, C., and Berry, J. A.: Linking chlorophyll a fluorescence to photosynthesis for remote sensing applications: Mechanisms and challenges, https://doi.org/10.1093/jxb/eru191, 2014.

Poulter, B., MacBean, N., Hartley, A., Khlystova, I., Arino, O., Betts, R., Bontemps, S., Boettcher, M., Brockmann, C., Defourny, P., Hagemann, S., Herold, M., Kirches, G., Lamarche, C., Lederer, D., Ottlé, C., Peters, M., and Peylin, P.: Plant functional type classification for earth system models: Results from the European Space Agency's Land Cover Climate Change Initiative, Geoscientific Model Development, 8, 2315–2328, https://doi.org/10.5194/gmd-8-2315-2015, 2015.

Qi, J., Chehbouni, A., Huete, A. R., Kerr, Y. H., and Sorooshian, S.: A modified soil adjusted vegetation index, Remote Sensing of Environment, 48, 119–126, https://doi.org/10.1016/0034-4257(94)90134-1, 1994.

Richiardi, C., Blonda, P., Rana, F. M., Santoro, M., Tarantino, C., Vicario, S., and Adamo, M.: A revised snow cover algorithm to improve discrimination between snow and clouds: A case study in gran paradiso national park, Remote Sensing, 13, https://doi.org/10.3390/rs13101957, 2021.

Roberts, D. R., Bahn, V., Ciuti, S., Boyce, M. S., Elith, J., Guillera-Arroita, G., Hauenstein, S., Lahoz-Monfort, J. J., Schröder, B., Thuiller, W., Warton, D. I., Wintle, B. A., Hartig, F., and Dormann, C. F.: Cross-validation strategies for data with temporal, spatial, hierarchical, or phylogenetic structure, Ecography, 40, 913–929, https://doi.org/10.1111/ecog.02881, 2017.

Rossini, M., Cogliati, S., Meroni, M., Migliavacca, M., Galvagno, M., Busetto, L., Cremonese, E., Julitta, T., Siniscalco, C., Morra Di Cella, U., and Colombo, R.: Remote sensing-based estimation of gross primary production in a subalpine grassland, Biogeosciences, 9, 2565–2584, https://doi.org/10.5194/bg-9-2565-2012, 2012.

Vicario, S., Adamo, M., Alcaraz-Segura, D., and Tarantino, C.: Bayesian Harmonic Modelling of Sparse and Irregular Satellite Remote Sensing Time Series of Vegetation Indexes: A Story of Clouds and Fires, Remote Sensing, 12, 83, https://doi.org/10.3390/rs12010083, 2019.

Wang, D., Liang, S., Zhang, Y., Gao, X., Brown, M. G., and Jia, A.: A new set of modis land products (Mcd18): Downward shortwave radiation and photosynthetically active radiation, Remote Sensing, 12, https://doi.org/10.3390/RS12010168, 2020.

Wang, L., Zhu, H., Lin, A., Zou, L., Qin, W., and Du, Q.: Evaluation of the latest MODIS GPP products across multiple biomes using global eddy covariance flux data, Remote Sensing, 9, https://doi.org/10.3390/rs9050418, 2017.

Wiltshire, A. J., Burke, E. J., Chadburn, S. E., Jones, C. D., Cox, P. M., Davies-Barnard, T., Friedlingstein, P., Harper, A. B., Liddicoat, S., Sitch, S., and Zaehle, S.: Jules-cn: A coupled terrestrial carbon-nitrogen scheme (jules vn5.1), Geoscientific Model Development, 14, https://doi.org/10.5194/gmd-14-2161-2021, 2021.

Yang, P., van der Tol, C., Campbell, P. K., and Middleton, E. M.: Fluorescence Correction Vegetation Index (FCVI): A physically based reflectance index to separate physiological and non-physiological information in far-red sun-induced chlorophyll fluorescence, Remote Sensing of Environment, 240, 111 676, https://doi.org/10.1016/j.rse.2020.111676, 2020.

Zhang, Y., Xiao, G., Wang, X., Zhang, X., and Friml, J.: Evolution of fast root gravitropism in seed plants, Nature Communications, 10, 4–13, https://doi.org/10.1038/s41467-019-11471-8, 2019.

https://doi.org/10.5194/egusphere-2023-2824
Preprint. Discussion started: 23 January 2024

Data availability.

The in situ data are available in the zenodo record https://zenodo.org/record/6428161

Appendix A: Appendix A

For the predictors included in the best performing model we also added a the scatter plot of each one against the variable of interest, splitting in 3 figures: radiance estimators in figure A4, meteo variables in figure A5 and finally spectral response in figure A6. Within this set of models the three types of estimated PAR are quite similar. The mean Av.LOO score for ssrd, ssrdXSVF and Radiance_Mod are 0.6424, 0.6309,0.6318, respectively. Given that ssrd estimate does not need DTM information and is marginally better than the other two estimates in this dataset, it is definitely the correct choice.

Author contributions. Concept : AP, MG, SV. *In situ* measurements: AP, MG, MM, GV. Data Analysis GPP: SV, MM, GV, CR. SV prepared the paper, and all authors contributed to the discussion and revision of the paper

Competing interests. the authors declare that no competing interests are present

Acknowledgements. We thank Ilaria Baneschi, Alice Baronetti, Maria Virginia Boiani, Angelica Parisi and Brunella Raco who have participated in the in-situ measurement campaigns, and Bruno Bassano, Ramona Viterbi and the GPNP technical personnel for logistic sup-

https://doi.org/10.5194/egusphere-2023-2824
Preprint. Discussion started: 23 January 2024

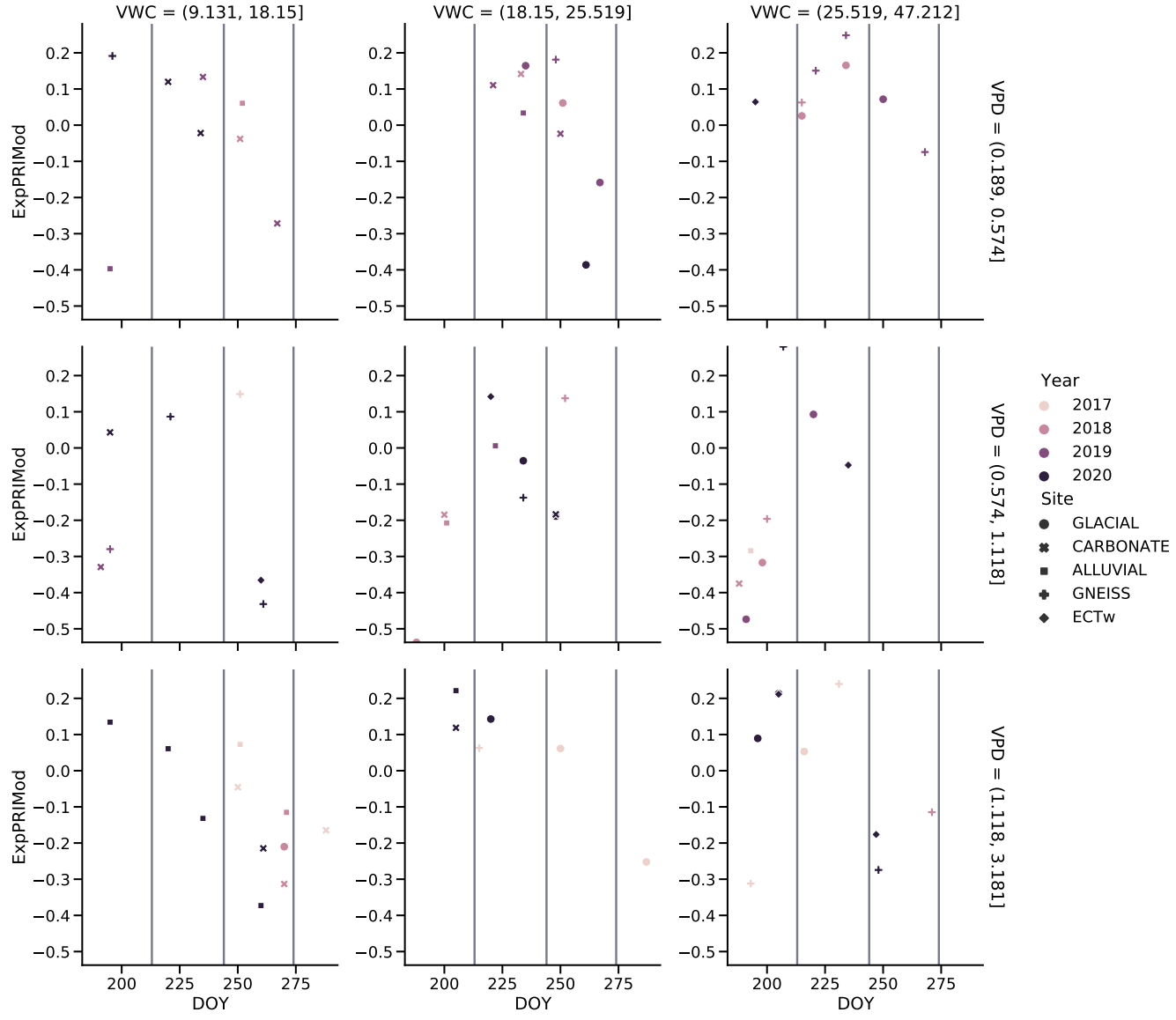

Figure A1. Measure of PRI as estimated by ExpPRIMod across time, expressed in Day of the year (DOY), splitting the observations in nine groups based 3 equinumerous bins on VWC and VPD values.

https://doi.org/10.5194/egusphere-2023-2824
Preprint. Discussion started: 23 January 2024

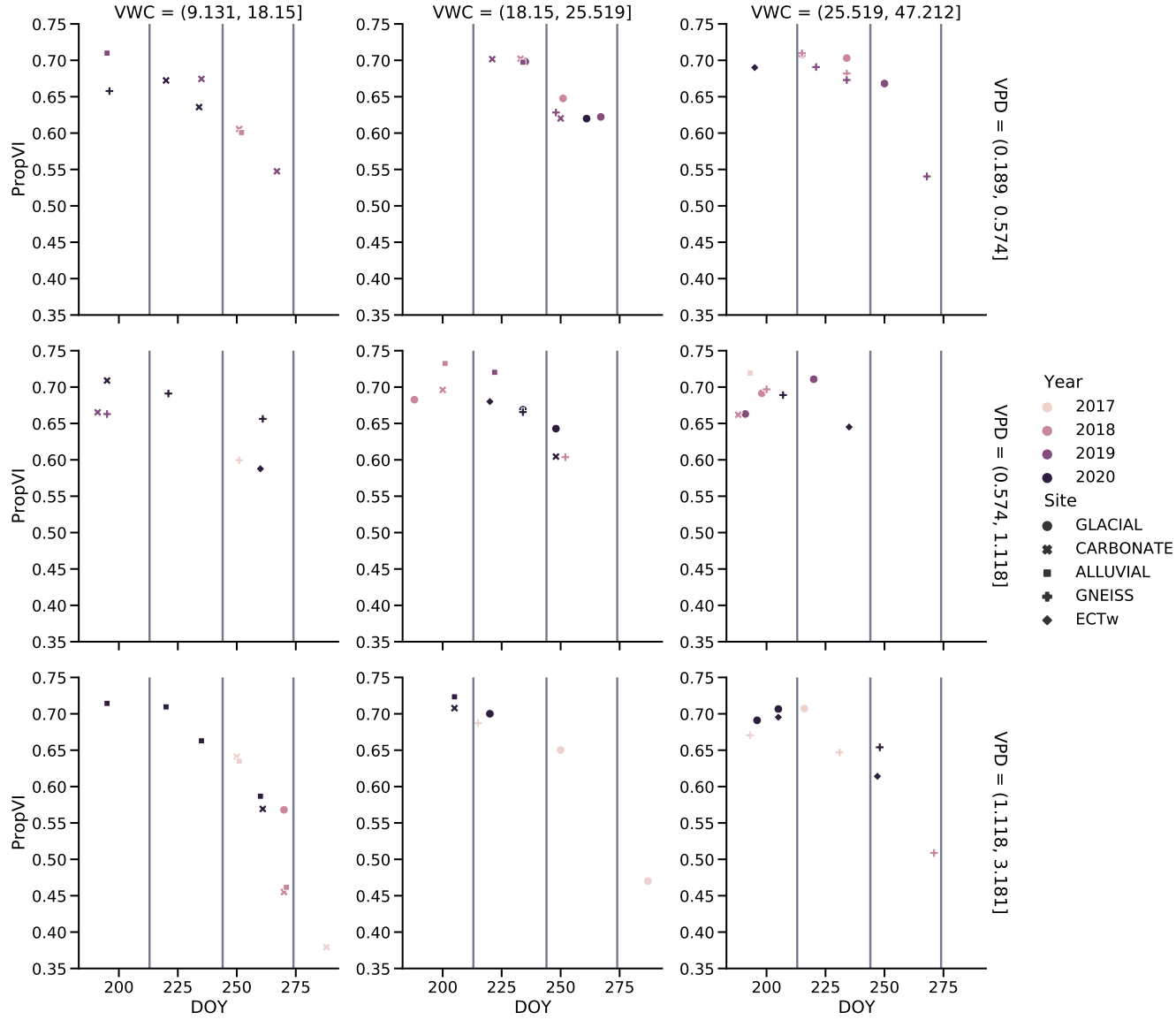

Figure A2. Measure of PropVI across time, expressed as Day of the year (DOY), splitting the observations in nine groups based on 3 equinumerous bins of VWC and VPD values.

https://doi.org/10.5194/egusphere-2023-2824
Preprint. Discussion started: 23 January 2024

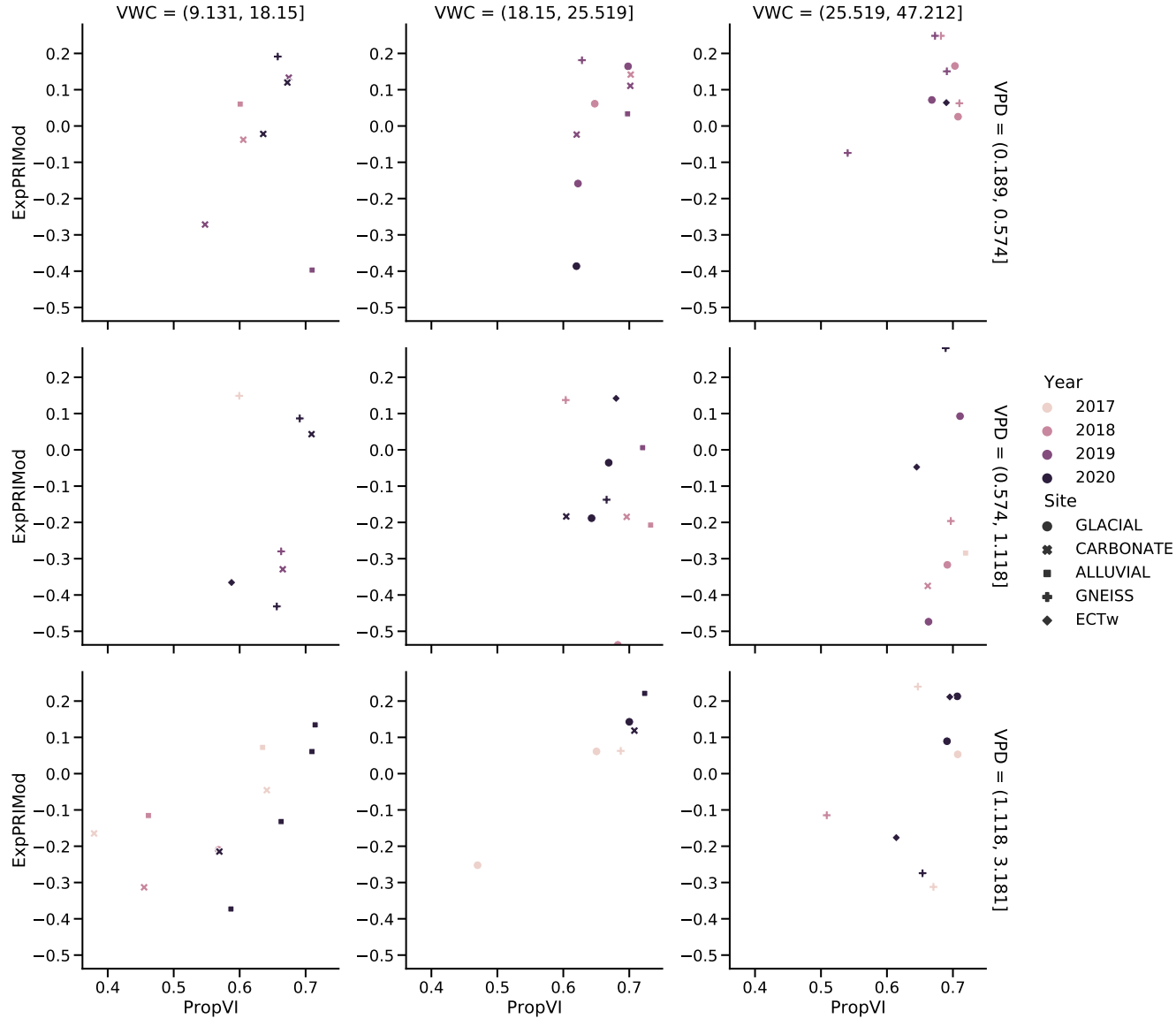

Figure A3. Scatterplot of PropVI and ExpPRIMod, splitting the observations in nine groups based on 3 equinumerous bins on VWC and VPD values.

https://doi.org/10.5194/egusphere-2023-2824
Preprint. Discussion started: 23 January 2024

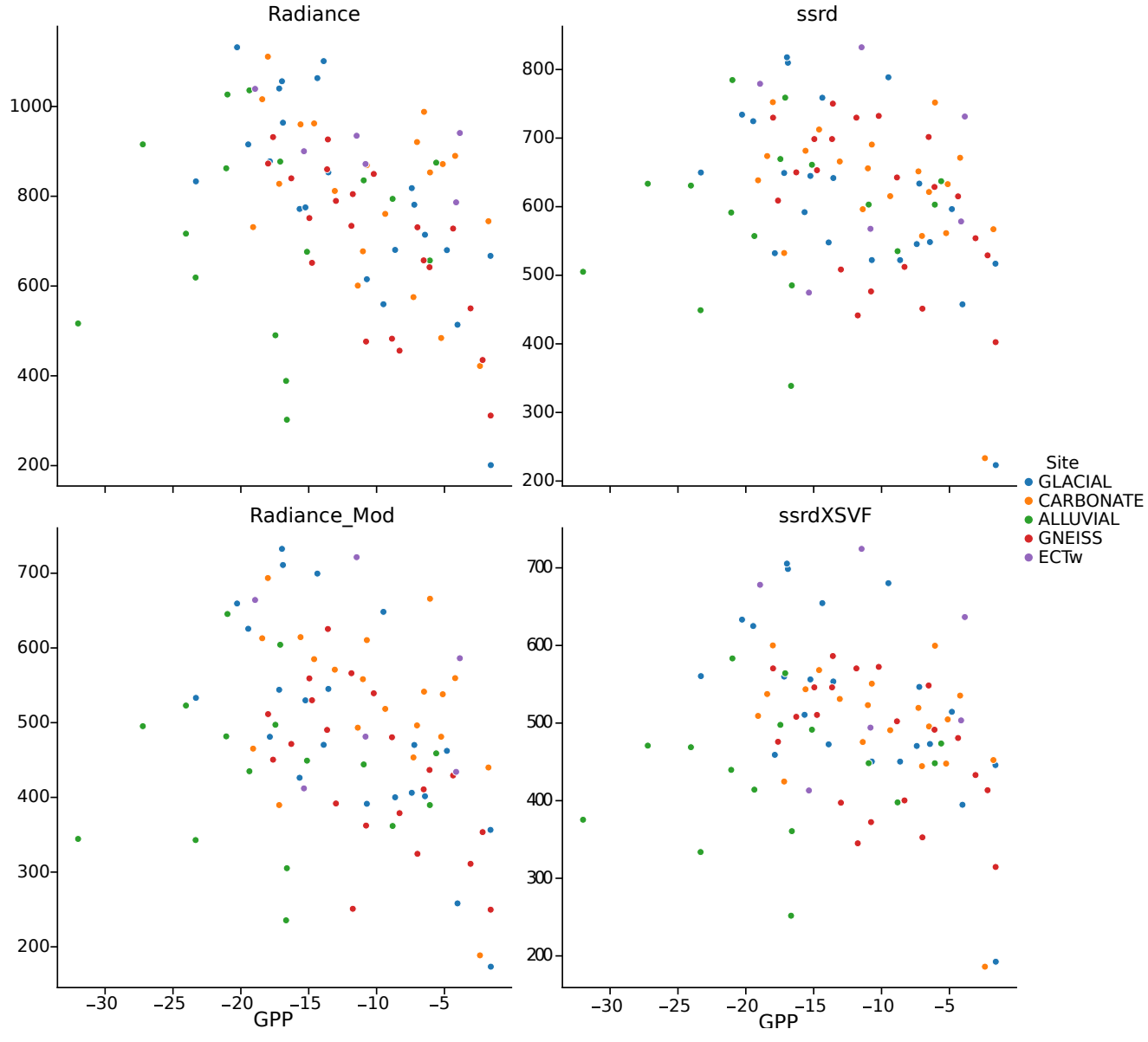

Figure A4. Relationship between in situ GPP and Radiance. The top left graph indicates in situ measure, while ssrd, Radiance_Mod and ssrdXSVF indicate 3 different estimates based on ERA5 reanalysis meteo model

https://doi.org/10.5194/egusphere-2023-2824
Preprint. Discussion started: 23 January 2024

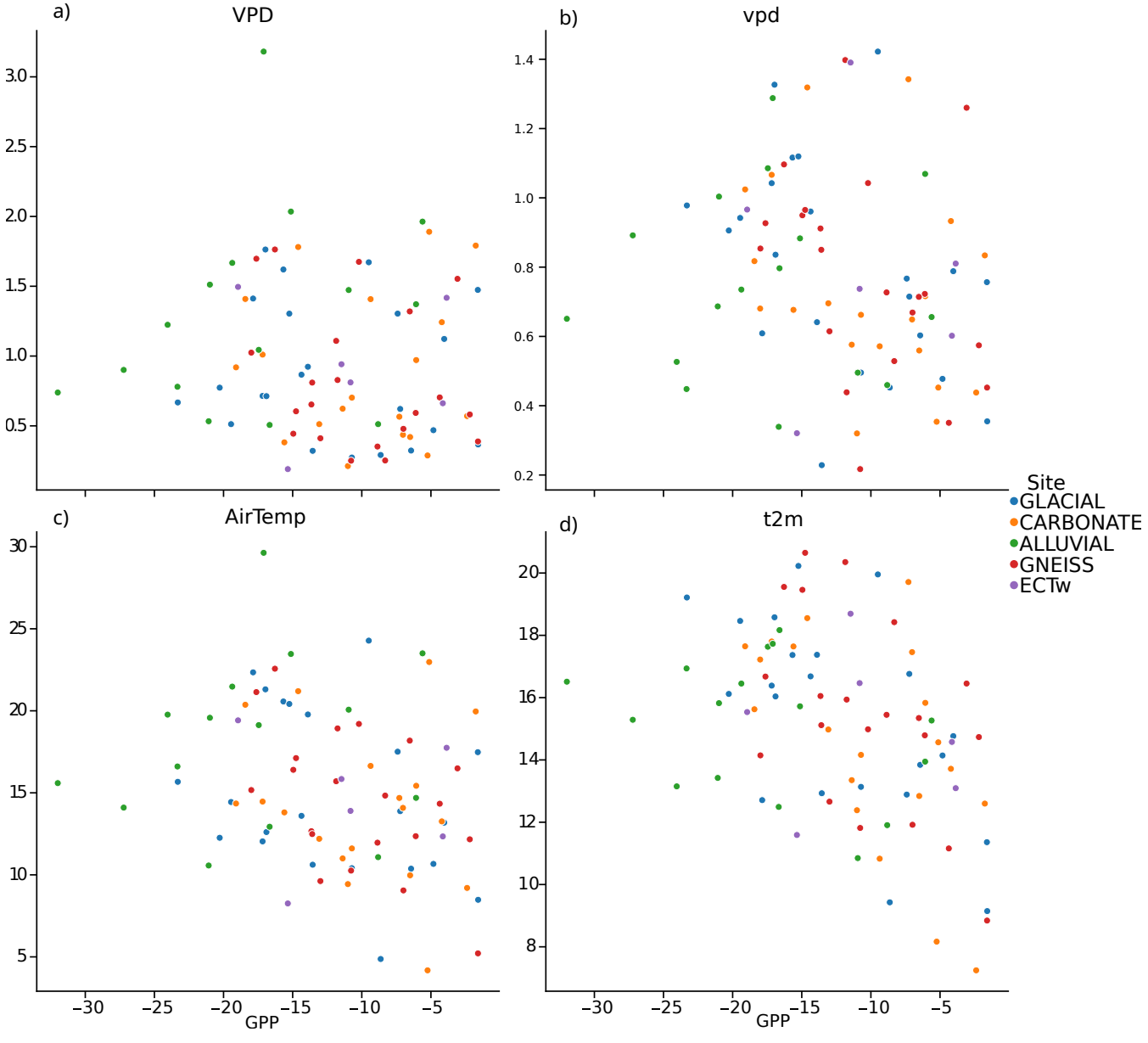

Figure A5. Relationship between in situ GPP and Meteo variables. (a), (b): using in situ meteo data; (c), (d): using ERA5-derived meteo variables.

https://doi.org/10.5194/egusphere-2023-2824
Preprint. Discussion started: 23 January 2024

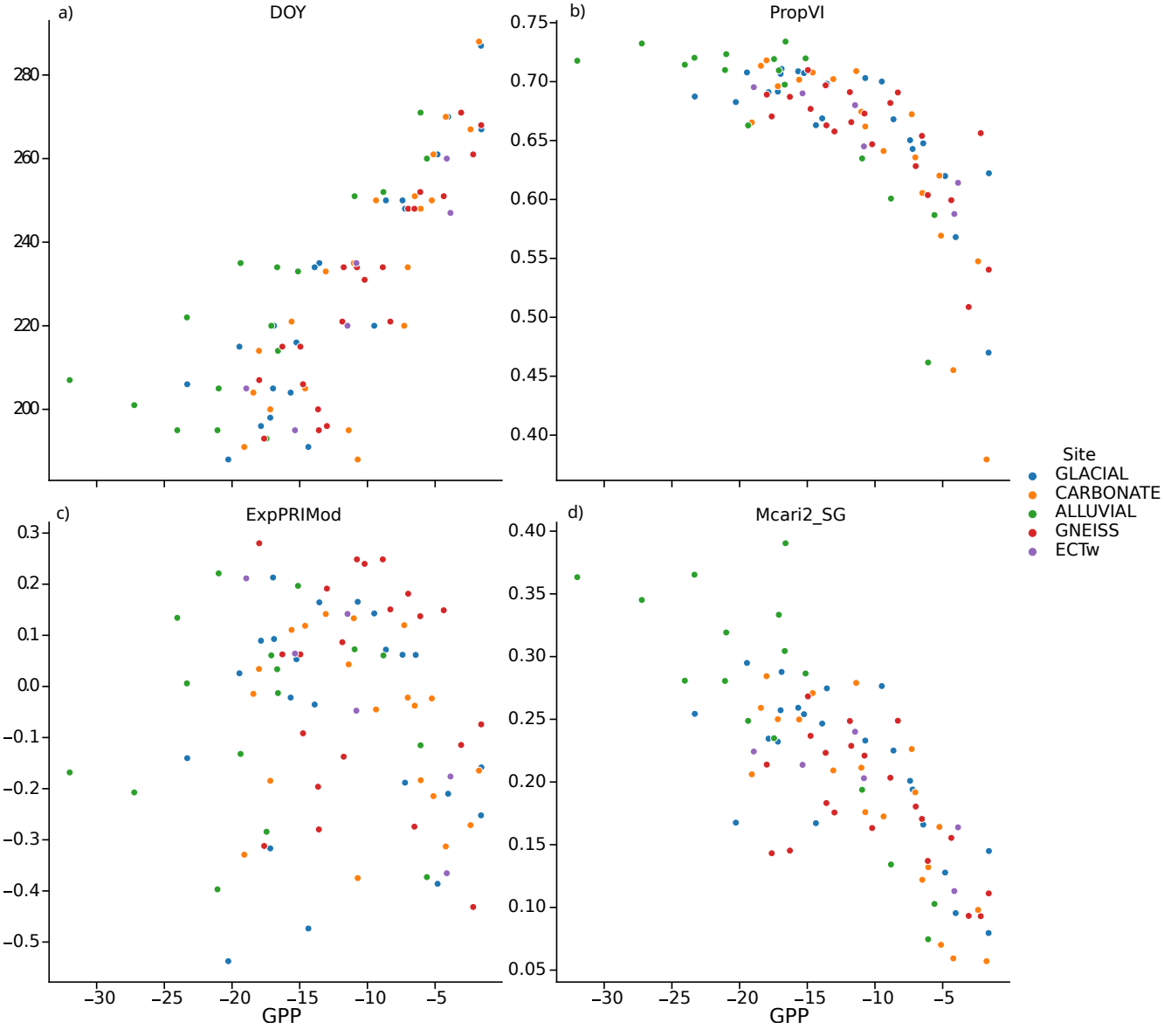

Figure A6. Comparing in situ GPP with Day Of the Year(DOY) and Satellite derived variables. from a) to d) graph represent comparison with DOY, time series corrected ratio of MCARI2 on MSAVI2 (PropVI), and PRI, MSAVI2

https://doi.org/10.5194/egusphere-2023-2824
Preprint. Discussion started: 23 January 2024

port. All authors acknowledge the funding by the H2020 projects e-SHAPE (grant agreement 820852) and eLTER plus (grant agreement 871128). M.M., A.P. e G.V. acknowledge support by the Italian National Biodiversity Future Center (NBFC) National Recovery and Resilience Plan (NRRP; mission 4, component 2, investment 1.4 of the Ministry of University and Research, funded by the European Union–NextGenerationEU; project code CN00000033)